Environmental fluctuations explain the universal decay of species-abundance correlations with phylogenetic distance

Matteo Sireci,[1,*] Miguel A. Muñoz,[1,†] and Jacopo Grilli[2,‡]

[1] *Departamento de Electromagnetismo y Física de la Materia e Instituto Carlos I de Física Teórica y Computacional. Universidad de Granada. E-18071, Granada, Spain*

[2] *Quantitative Life Sciences, The Abdus Salam International Centre for Theoretical Physics, 34151 Trieste, Italy*

Multiple ecological forces act together to shape the composition of microbial communities. *Phyloecology* approaches —which combine phylogenetic relationships with community ecology— have the potential to disentangle such forces, but are often hard to connect with quantitative predictions from theoretical models. On the other hand, *macroecology*, which focuses on statistical patterns of abundance and diversity, provides natural connections with theoretical models but often neglects inter-speficic correlations and interactions. Here, we propose a unified framework combining both such approaches to analyze microbial communities. In particular, by using both cross-sectional and longitudinal metagenomic data for species abundances, we reveal the existence of a novel empirical macroecological law establishing that correlations in species-abundance fluctuations across communities decay from positive to null values as a function of phylogenetic similarity in a consistent manner across ecologically distinct microbiomes. We formulate three mechanistic models —relying on alternative ecological forces— that lead to radically different predictions. We conclude that the empirically observed macroecological pattern can be quantitatively explained as a result of shared fluctuating resources, i.e. *environmental filtering* and not e.g. as a consequence of species competition. Finally, we also show that the macroecological law is also valid for temporal data of a single community, and that the properties of delayed temporal correlations are reproduced by the model with environmental filtering.

Microbial communities are ubiquitous on earth, from human microbiota, to ocean, soil, and glacial environments [1]. Their widespread presence is paralleled by their complex and highly variable composition, both across time and space [2]. Understanding what are the main drivers, or *"ecological forces"*, shaping the coexistence and stability of microbial communities under changing environmental conditions and perturbations, is a fundamental challenge of utmost relevance for e.g. environmental and health sciences.

Ecological forces can emerge from the interaction between species or between species and the environment, including both biotic and abiotic factors. Experiments in simple and controlled laboratory environments have made it possible to trace the effects of various ecological forces on community composition, often reshaping classical ideas on ecological interactions [3–7]. For instance, "cross-feeding" has emerged as a central player in determining community assembly and species coexistence [8, 9]. However, the role of different ecological forces in determining composition and variation in more complex natural communities remains mostly unknown. While detailed information about environmental [10–

*Electronic address: msireci@onsager.ugr.es
†Electronic address: mamunoz@onsager.ugr.es
‡Electronic address: jgrilli@ictp.it

12] and genetic [13–15] factors shaping interaction and response to environmental conditions is sometimes available, we still lack frameworks to infer their quantitative strength and to disentangle the relative relevance of each of the acting ecological forces from available data[16–18].

Macroecology —i.e. the study of ecological communities through the analysis of global patterns of abundance, diversity, and distribution [19]— stands as a prominent approach to link quantitative ecological models with empirical data of complex and diverse communities [20, 21].

In the context of microbial communities, a growing body of evidence shows that the abundance dynamics observed in microbial communities is characterized by distinctive and reproducible statistical patterns, also known as *macroecological laws* [21–25]. Further evidence shows that, despite the complexity of the underlying microscopic dynamics, most of such patterns can be reproduced by relatively simple models —such as e.g. the stochastic logistic model (SLM)— capturing salient features of the underlying ecological forces [22–26]. However, such simplified models often neglect the interactions between species, treating their abundance fluctuations as independent from each other. Nevertheless, it is noteworthy that including species interactions in the SLM model does not significantly affect the shape of single-species macroecological patterns; for instance, generalized Lotka-Volterra equations with environmental stochasticity —which reduce to the SLM in the absence of interactions— predict time-series statistics and patterns similar to the SLM [23–25].

On the other hand, the ecological forces shaping community composition and variability can only be unveiled within the macroecological approach by explicitly studying multispecies abundance patterns. For instance, empirically-determined pairwise correlations between species abundances can be partially explained by consumer-resource models with resource fluctuations [26].

One challenge in connecting macroecological patterns with simple yet biologically-grounded models is that not all statistical patterns are equally informative. For instance, it is well known that, in many ecological systems, the empirical shape of the species abundance distribution (SAD) —i.e. one of the most prominent macroecological patterns— can be reproduced by models with very different underlying biological assumptions (such as, e.g. neutral and niche theories [27, 28]). Similarly, multiple mechanisms are expected determine the observed correlations between species abundance fluctuations. These correlations are in fact the result of multiple ecological forces, such as competition, cooperation, cross-feeding, but also of indirect effects through a network of interactions [29]. Analyzing the phylogenetic structure of community composition [30, 31] is a standard approach to disentangle the effects of these alternative assembly mechanisms. This type of approach is generally applied to analyze species (co-)occurrence: e.g. shared environmental fluctuations (called "*environmental filtering*" hereon) produce phylogenetic clustering (similar species share a tendency to be simultaneously present or absent [32]), while exclusion by limiting similarity determines phylogenetic overdispersion (similar species tend not to be simultanbeously present). These approaches have been widely applied in plant communities but also in other systems [33–35] including microbial communities [36]. More generally, phyloecology, which combines phylogenetic relationships with community ecology, has the potential to reveal the processes determining community composition [37]. However, with few notable exceptions focusing on testing neutral models [38, 39], a connection between empirical observations of community ecology based on phylogeny and quantitative predictions of theoretical models is still missing.

Here, our goal is to develop such a connection under the lens of macroecology. In particular, we first elucidate the existence of a new empirical macroecological law that associates pairwise abundance correlations with species

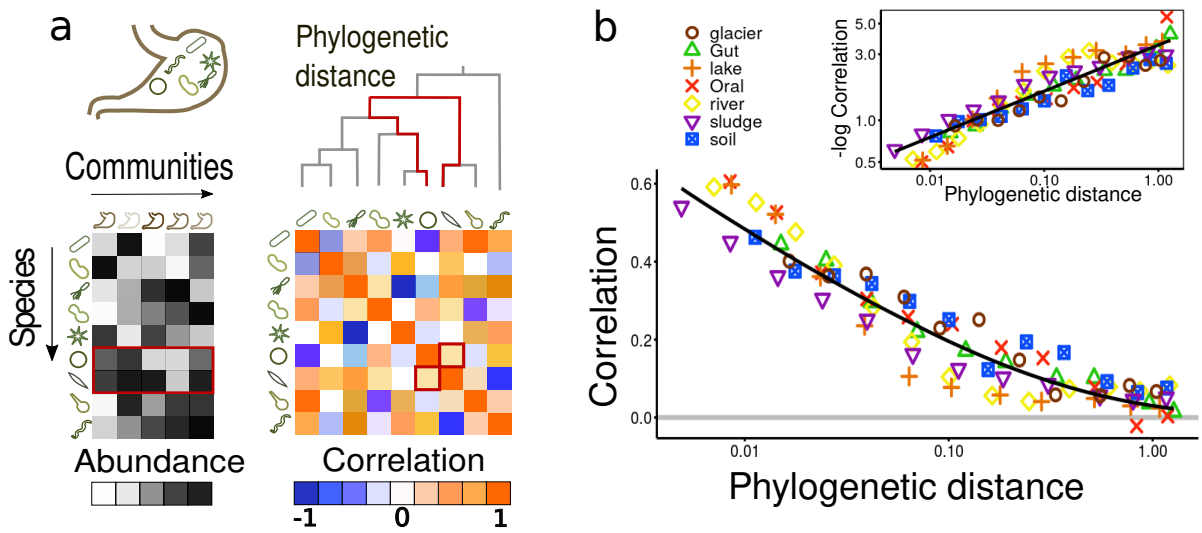

FIG. 1: (a) Pictorial illustration of the data organization and statistical analyses. Abundances of different species (i.e. OTU at 97% similarity [40]), for different communities of the same biome (e.g gut of different hosts) are collected, respectively in rows and columns of the left table. The grey scale in the matrix entries stands for the level of abundance with darker shades corresponding to more abundant species. The (symmetric) species-abundance correlation matrix (color coded) is obtained by calculating for each pair of existing species the correlation of abundance fluctuations across communities. Finally, the phylogenetic distance is computed for all possible pairs of species by reconstructing the phylogenetic tree; and than associated with the couple correlation. The abundances, correlation, and phylogenetic distance of two given species are emphasized in red color. **(b) Macroecological law for pairwise correlations as a function of the phylogenetic distance for different biomes.** The correlation of abundance fluctuation averaged over all couples within a given discretized distance bin (colored symbols) decays with the phylogenetic distance (log scale) for all the considered microbiomes (see legend). In particular, each bin in the x-axis includes all couples with a phylogenetic distance within such a discrete bin (each one including at least 10^3 couples for each of the 8 considered biomes; as shown in the SI, the pairs are not uniformly distributed across phylogenetic distances: the vast majority of couples lie in the rightmost bins, with large distances and small pairwise correlation values). The black line represents a stretched-exponential decay, Eq.(1) with $\lambda \approx 3.5$. To emphasize the functional dependence, the inset shows the same data but for the negative log of the correlations represented in double logarithmic scale (i.e., a plot in which stretched exponential functions become straight lines; in this case with slope 1/3).

phylogenetic similarity. To rationalize such a finding, we formulate three alternative theoretical models —each relying on different ecological forces— all of which reproduce previously studied single-species macroecological patterns [23–25], but lead to radically different predictions for phylogenetic-dependent correlation patterns. These analyses allow us to conclude that only *environmental filtering* (and not, e.g., species competition) explains the empirically-observed pattern of decaying correlations with phylogenetic distance. Last but not least, we analyze temporal data for a fixed community, showing that the macroecological law also holds quantitatively in this context and that delayed temporal correlations are naturally reproduced by our model with environmental filtering.

Results

The averaged correlation of abundance fluctuations decays with phylogenetic distance in a consistent fashion

We consider the phylogenetic (or "cophenetic") distance, $d_{G,ij}$ (where the subindex G stands for "genetic") for each pair of operational taxonomic units (OTUs) (i, j), by using publicly-available results from $16S$ ribosomic RNA metagenomic analyses [40, 41]. This genetic distance exhibits a broad variability across OTU pairs (see Methods and Fig. S1). For each pair of OTUs, we also measure the correlation between the correponding abundance fluctuations η_{ij} (see Fig. 1(a) and Methods) across samples. Fig. 1(b) illustrates the typical value of the pairwise correlation η, averaged over the pairs of OTUs at a given phylogenetic distance (where distances are grouped in discrete intervals or bins). The resulting averaged correlation decays with the phylogenetic distance d_G in a robust way across environments and datasets. In particular, phylogenetically close OTUs (small values of d_G) display a significant positive correlation while, for distant OTUs, the correlation decreases to zero and becomes statistically indistinguishable from the one between two randomly selected OTUs. Conversely, the positive correlations at low phylogenetic distances are significantly higher than the ones measured in randomized-data, obtained by shuffling the position of OTUs on the phylogenetic tree. We confirmed the robustness of this empirical observation by changing the metric to quatify abundance pairwise correlations, obtaining in all cases similar decaying correlation patterns (SI Fig. S2-S3).

At a more quantitative level, the reported decay of the correlation function is well captured by a stretched-exponential function [42]:

$$\eta(d_G) = e^{-\lambda d_G^{1/3}} \ , \tag{1}$$

as shown in Fig. 1(b). Interestingly, the decay of the correlation function is slower than exponential: the logarithm of the correlations exhibits an algebraic (power-law) scaling with the phylogenetic distance d_G as explicitly illustrated in the inset of Fig. 1(b).

In order to scrutinize whether the observed pattern is consistent across the phylogenetic tree, we repeated the same type of analyses at the coarser level of taxa, comparing correlations within and between taxonomic orders. Fig. S7 shows that species from different taxa (i.e. at large phylogenetic distances) tend to have, on average, zero correlation, while the averaged correlations within the same taxa decay from positive to zero with phylogenetic distance, recovering the pattern in Fig. 1 in a consistent way in the vast majority of the observed taxa (see Fig. S8).

These results suggest that the observed correlation pattern showing a stretched-exponential decay with phylogenetic distance is a universal one, not depending on the considered ecological context nor on a particular taxa. Whatever ecological forces are at the origin of such species abundance correlations, they manifest themselves regularly and consistently in diverse taxa and biomes.

Ecological forces in preference space: three alternative scenarios produces three alternative predictions

Which ecological forces are responsible for the described pattern of correlations of species abundances fluctuations across communities? In general, complex patterns of interactions in a network of species could *a priori* create both positive and negative correlations, also as the result of indirect or network effects.

To unravel these conflicting mechanisms, we consider a general population-dynamics model where species grow and compete for resources in a fluctuating environment. To be more specific, we consider a set of N species whose growth is coupled with a set of R available resources and M other abiotic factors (such as temperature, pH, salinity, etc.). We assume that all these $R+M$ factors are characterized by independent temporal fluctuations. The fundamental difference between the two sets, is that resources are also affected by population abundances through consumption, while abiotic factors are not. We assume that the effect of the environment on a given species can be represented as a vector in an abstract high-dimensional $(R+M)$ trait space. Such an ecological trait space represents the preferences for the R available resources and growth responses to the M abiotic factors. Thus, the set of resource preferences of any given species i is represented by a vector $\boldsymbol{b}^i$ in an abstract R-dimensional space of resources (see Fig. 2 (a) for a pictorial illustration). Similarly, the preferences for abiotic factors are represented by the vector $\boldsymbol{a}^i$ in a M-dimensional space. For simplicity, and without loss of generality, we assume that all these vectors are normalized to one.

The per-capita growth rate of each species is influenced both by resources consumption and abiotic environmental factors, both weighted by the corresponding preferences vectors, leading to the following general model

$$\frac{1}{x_i(t)}\frac{dx_i}{dt} = \sum_{\beta=1}^{R} b^i_\beta R_\beta(t) + \sum_{\alpha=1}^{M} a^i_\alpha M_\alpha(t) - \delta \ , \tag{2}$$

where $x_i(t)$ is the abundance of species i at time t, $R_\beta(t)$ is the abundance of resource β at time t, $M_\alpha(t)$ is the time-dependent value of the abiotic factor α, and δ is a constant death rate. We assume the abiotic factors to be subject to stochastic fluctuations

$$M_\alpha(t) = \bar{M}\left(1+\sqrt{\nu}\zeta_\alpha(t)\right) \ , \tag{3}$$

where $\bar{M}$ represents a baseline level, $\zeta_\alpha(t)$ is a (zero-mean unit-variance) Gaussian white noise and the parameter ν quantifies the strength of fluctuations. Similarly, the abundance R_β of each resource β fluctuates over time. The abundance is determined by a balance between stochasticity and consumption, i.e.,

$$R_\beta(t) = \bar{R}\left(1+\sqrt{\omega}\varphi_\beta(t) - \gamma\sum_{j=1}^{N} b^j_\beta x_j\right), \tag{4}$$

where $\bar{R}$ is a baseline level, γ the consumption timescale, $\varphi_\beta(t)$ a (zero-mean unit-variance) Gaussian white noise, and the parameter ω quantifies the amplitude of fluctuations.

The model defined in Eq.(2) can be *effectively* written as a generalized Lotka-Volterra model with fluctuating growth rate and species competition

$$\frac{dx_i}{dt} = x_i\left(\bar{r}_i + \sqrt{\sigma}\xi_i(t) - \sum_{j=1}^{N} C_{ij}x_j\right) \ , \tag{5}$$

where $r_i(t) = \bar{r}_i + \sqrt{\sigma}\xi_i(t)$ is a time-dependent and fluctuating growth rate, with mean value $\bar{r}_i$, and the entries of the competition matrix, C_{ij}, are determined by the overlap in resource preference of species i and j

$$C_{ij} = \bar{R}\gamma\ \boldsymbol{b}^i\cdot\boldsymbol{b}^j, \tag{6}$$

and noise covariances are $\langle\xi_i(t)\xi_j(t')\rangle = \rho_{ij}\delta(t-t')$ with

$$\rho_{ij} = \frac{\nu\bar{M}^2\boldsymbol{a}^i\cdot\boldsymbol{a}^j + \omega\bar{R}^2\boldsymbol{b}^i\cdot\boldsymbol{b}^j}{\nu\bar{M}^2+\omega\bar{R}^2}. \tag{7}$$

The explicit dependency of $\bar{r}_i$, σ and ξ_i on the original parameters is described in the Methods section. Observe that growth-rate correlations depend both on resources and abiotic factors ($\boldsymbol{b}$ and $\boldsymbol{a}$) while the effective competition is mediated only by shared resources ($\boldsymbol{b}$) as abiotic factors are not limiting.

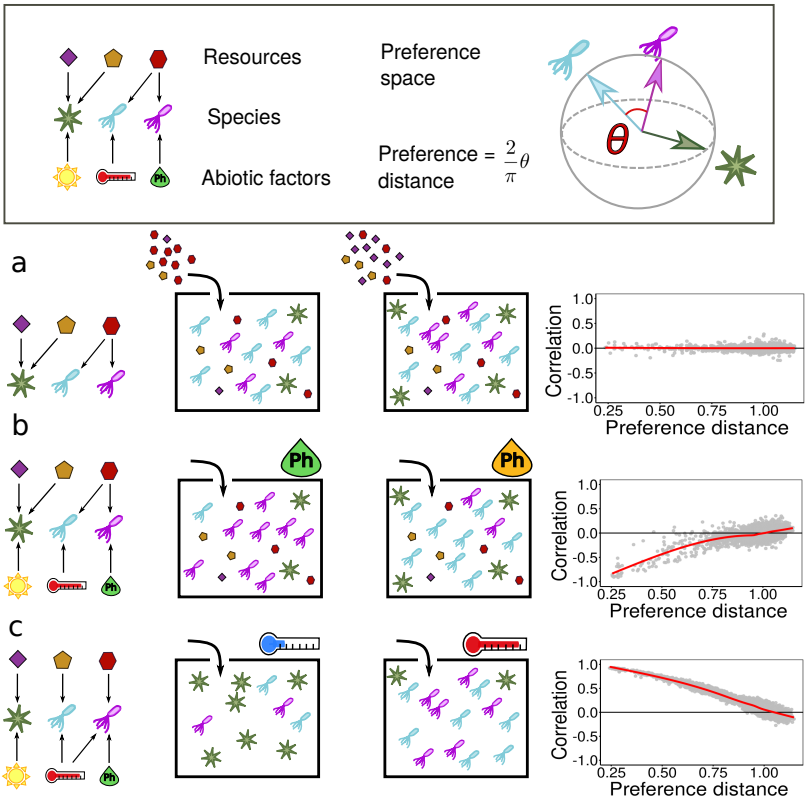

FIG. 2: (Top) Sketch of the elements of the model. *Left:* Bacterial species depend upon both *biotic factors* such as resource abundances (polygons) and *abiotic environmental factors* (e.g. temperature, ph, light intensity, etc.). The arrows stand for species preferences. *Right:* Species preferences are represented as radial vectors in a sphere: positive/negative projections represent positive/negative influence on growth. The (pairwise) preference distance is quantified by the angle between vectors (multiplied by $2/\pi$, see methods). The red and blue species are similar to each other while the green one is more different from them. **(Bottom) Schematic illustration for the three considered scenarios** (models A, B and C) of: (*left*) biotic and abiotic preferences; (*centre*) model dynamics, and (*right*) stationary correlations as a function of preference distance (with gray dots standing for simulation results and red lines for averages/theory). **(a) Shared fluctuating resources with fixed abiotic factors.**When species are subjected to the combination of both forces, their effects cancel out leading to an "effective" neutral situation with no correlations. **(b) Shared resources and non-overlapping fluctuating abiotic factors.** when two species sharing some resource preference experience an environmental fluctuation, one outcompetes the other, causing negative correlations, increasing monotonically to zero as similarity decreases. **(c) Shared fluctuating abiotic factors with fixed non-overlapping resources.** If two species share some preference for abiotic factors, but not for resources, the follow in a similar way environmental fluctuations, causing positive correlations which decrease with preference distance.

Thus, both of the coupling terms in the effective Lotka-Volterra population dynamics —i.e. the species competition matrix and the growth-rate fluctuation covariance matrix— crucially depend on the set of species similarities in preference space. However, depending on the relative strength of both types couplings as well as on the distribution

of preferences vectors, one can define three different models, depending on which are the dominating ecological forces (see Fig.2 a/b/c):

(A) *Shared fluctuating resources with fixed abiotic factors.*
If abiotic fluctuations are negligible (i.e. $\nu = 0$), species interactions are determined by a combination of the effect of competition (encoded in the entries C_{ij}) and resource fluctuations (encoded in the entries ρ_{ij}), which are both proportional to the species resource-preference overlap: $\boldsymbol{b}^i \cdot \boldsymbol{b}^j$.

B) *Shared resources and non-overlapping fluctuating abiotic factors.*
If resource fluctuations are negligible (i.e., $\omega = 0$) and abiotic factors preferences are all orthogonal to each other, species experience independent growth rate fluctuations ($\rho_{ij} = \delta_{ij}$) and competition for fixed resources (through the coupling matrix C_{ij}).

(C) *Shared fluctuating abiotic factors with fixed non-overlapping resources.*
If resource preferences are all orthogonal to each other, there are, essentially, no shared resources. In this case, species experience correlated growth rate fluctuations and no inter-specific competition $C_{ij} = \bar{R}\ \gamma\ \delta_{ij}$. We refer to this force as "*environmental filtering*".

More complex models involving involving both correlated abiotic and resource fluctuations could also be constructed, but, for the sake of clarity, here we focus of these three (simplest) ones.

Using extensive numerical simulations (see Methods) we investigate the relationship between pairwise abundance correlations and preference similarities for the three models. In particular, one can define a preference distance, d_P, proportional to the angle between preference vectors (with $d_P = 0$ for coinciding vectors and $d_P = 1$ for orthogonal ones). In model (A) and (B) the distance is calculated over the resource preference $\boldsymbol{b}$, while the vectors of abiotic preferences $\boldsymbol{a}$. are considered in model (C).

As illustrated in Figure 2(a/b/c) the three models give raise to three qualitatively distinct patterns of correlation as a function of preference distance d_P. (A) Shared fluctuating resources with fixed abiotic factors induce an effective *neutral* behavior, with nearly vanishing correlations across the spectrum of pairwise preference distances. (B) Shared resources and non-overlapping fluctuating abiotic factors produce *negative* correlations at small distances that increase to near-zero values in a monotonic way. (C) Shared fluctuating abiotic factors with fixed non-overlapping resources lead to correlations decaying from *positive* to vanishing values with distance.

Environmental filtering reproduces the correlation decay with distance.

In order to make a more quantitative comparison between the previous results and the empirically-determined universal pattern of decaying correlations, it is necessary to specify the relation between the preference distance d_P — on which the models rely— and the empirically-determined phylogenetic similarity of actual species, as quantified by their genetic distance d_G. For this purpose, it seems natural to assume that d_P and d_G are positively correlated, i.e., that phylogenetically close species typically have more similar preferences than distant ones. Under this assumption, the overall trend of the decay in Fig. 2 implies that environmental filtering is the process responsible for the empirically-observed decay of correlations (Fig. 1). Competition for constant and/or shared fluctuating resources can instead be

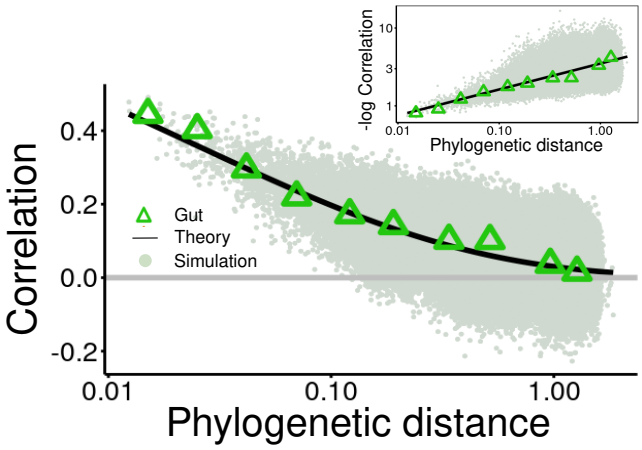

FIG. 3: The model with environmental filtering reproduces the empirical law. Correlation values are plotted as a function of the phylogenetic distance both for the gut microbiome data (green triangles for each binarized value) and the simulated computational model (green clouds of points). The analytical expression, eq.(1), with $\lambda = 3.5$ is also plotted (black line). The independent simulations of the model have been performed, using $N = 300$ species and considering as an input the empirical phylogenetic distance matrix of the gut microbiome, randomly sampling from it N species. Inset: -log Correlations vs phylogenetic distance in log-log scale, empirically and from the mode, same data as the main figure. For more simulations details see Methods

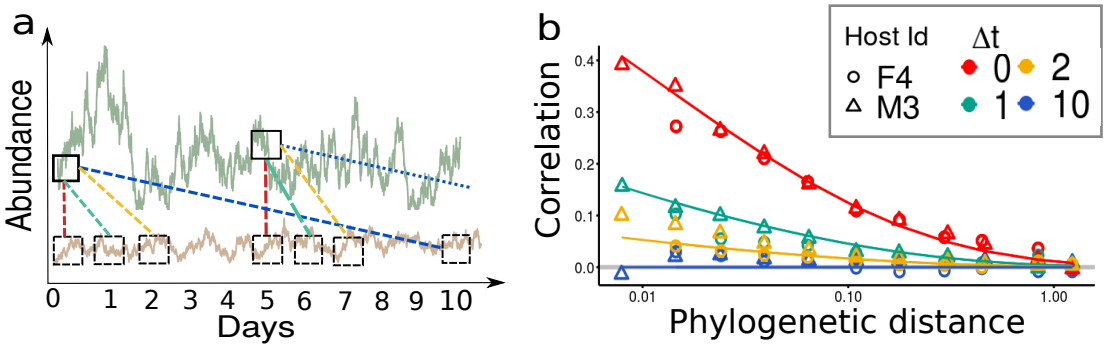

FIG. 4: (a) Sketch of the time-dependent (longitudinal) correlation data analyses. Typical time-series for two species (green and brown, respectively) along 10 days. The dashed lines illustrate how equal-time (red) and $1, 2, 10$ days delayed correlations (green, yellow and blue respectively) are computed, see Methods for more details. **(b) Macroecological law for temporal data**. Equal time (red), one-day delay (light blue), two-days (yellow) and ten-day delay (blue) symbols represent correlations as a function of the discretized phylogenetic distance (logarithmic scale) for the gut microbiomes of two different hosts (labelled with circles (F4) and triangles (M3), respectively). Solid lines stand for the prediction from the CSLM, Eq.(45), averaged over hosts, with timescale parameter $\tau_i = 1$, for $i = 1, .., N$ and $\lambda = 4.5$.

discarded as the leading mechanism on the basis of the empirically observed pattern. This does not imply that competition is not present, but rather that it does not generate a signal detectable at a phylogenetic level within the present level of resolution.

To make further quantitative progress in the connection between the previous mechanistic modelling approaches

—in particular, model C or "environmental filtering"— and available phylogenetic data, one needs to define a more precise mapping between preference similarity in the model and empirically-determined phylogenetic distance, i.e. to characterize the functional dependence between d_P on d_G, using information on pairwise correlations.

The previous task is not straightforward at all: species are coupled to each other, so that pairs of species cannot be simply analyzed one at the time and, on the other hand, the full set of coupled non-linear equations is intractable. However, as explicitly shown in the Methods section we can make further progress by assuming that the the preference space has a large dimensionality, i.e. $M \gg 1$. In this limit it becomes possible to explicitly map model C into a *correlated stochastic logistic model* (CSLM) (see Methods for a detailed derivation):

$$\frac{dx_i}{dt} = \frac{x_i}{\tau_i}\left(1 - \frac{x_i}{K_i}\right) + \sqrt{\frac{\sigma_i}{\tau_i}} x_i \xi_i(t), \tag{8}$$

where τ_i^{-1} is the growth rate, K_i the carrying capacity, σ_i the amplitude of environmental fluctuations, and $\xi_i(t)$ is a Gaussian white noise, with correlations proportional to the preference distance,

$$\langle \xi_i(t)\xi_j(t')\rangle = \cos\left(\frac{\pi}{2} d_{P,ij}\right). \tag{9}$$

This mapping is particularly illuminating as the resulting CSLM extends the standard stochastic logistic model (SLM) [23], as it includes correlated growth-rate fluctuations that stem from shared environmental noise and that induce non-trivial species correlations. Moreover, it is important to stress that —if species-abundances trajectories are observed individually— there are no statistical differences between the CSLM and the standard SLM. This implies that the CSLM also reproduces (as the SLM does) the three macroecological patterns put forward in [23–25] (see Methods). Thus, the CLSM constitutes an improvement of existing modelling approaches to microbial macroecological laws.

Another advantage of Eq.(8) (together with and Eq.(9)), is that is can be treated analytically to obtain a mathematical expression linking pairwise species-abundances correlations with their preference distance, $d_{P,ij}$ (see Methods). The resulting analytical relationship can be exploited to estimate the preference distance matrix from empirical correlation data, thus allowing us to establish the desired relation between preference distance d_P and phylogenetic distance d_G (see Methods):

$$d_{P,ij} \approx \frac{2}{\pi} \arccos\left(e^{-\lambda d_{G,ij}^{1/3}}\right), \tag{10}$$

where λ is a constant. Observe, that Eq.(10) is highly non-linear, implying that, as the phylogenetic distance grows, preference distances rapidly saturate to values close to 1; in other words, even phylogenetically similar species tend to have a large preference dissimilarity (i.e. their preference vectors tend to be orthogonal to each other).

By implementing the relation (10) in the definition of noise correlations Eq.(9), we obtain a version of the CSLM, directly relating ecological processes and phylogeny, which allows us to relate the species-abundance correlations to their empirically measured genetic similarity. Actually, given that the macroecological pattern we intend to reproduce is for the averaged correlation at a given (binarized) phylogenetic distance, we dropped the sub-index ij in Eq.(10) and use it as a relation between averages (see Methods, Eq.(46)). In particular, by combining Eq.(46) and Eq.(37) in Methods, one obtains exactly Eq.(1), i.e. the empirically observed relation between correlation and phylogenetic distance.

Fig. 3 shows that, for the particular case of the human gut microbiome, a computational simulation of this model captures rather well the averaged decay of pairwise correlations with phylogenetic distance and that the analytical predictions describe quite well such an averaged behavior.

The macroecological law holds for temporal (longitudinal) data

One important prediction of Eq.(8) is that the decay of abundance correlations with phylogenetic distance is caused by shared temporal fluctuations. In order to further test the predictions of Eq.(8), we consider longitudinal data from the human microbiome. In particular, we analyzed three human body sites (gut, oral cavity, and hand palms) of two hosts [41]. From these data, we calculate the correlation of species abundance fluctuation η_{ij} as done above, but now averaging over time, rather than across communities (see Fig. 4(a)). Figure 4(b) illustrates —for the specific case of the human gut— that the macroecological law of correlation holds also for such temporal data, and that delayed correlations rapidly decay to zero. In particular, the correlations as a function of phylogenetic distance still decay on average as a stretched exponential with exponent 1/3, as observed in cross-sectional data.

To further test the CSLM model in its ability to reproduce time-dependent features of species correlations, we also computed delayed pairwise correlations, $\eta_{ij}(\Delta t)$ defined as the correlation between the abundance fluctuations of species i at time t with the abundance fluctuations of species j at time $t + \Delta t$ (see Methods and Fig. 4 (a) for a graphical illustration). Let us remark that, in principle, the value of such a delayed correlation is, in general, not trivially linked to the correlation computed at the same time, as it depends of the specific properties of the dynamics giving rise to species interdependences. Remarkably, as shown in Figure 4(b) the CSLM with no additional modification quantitatively reproduces also the temporal delayed correlations for different values of the delay in two microbiomes (see SI for additional details and analyses) only by tuning the growth time scale $\tau_i = 1$ for all species.

Discussion

We have considered both cross-sectional and longitudinal empirical data for the species abundances in microbial communities from many different environments and studied their patterns of species-abundance pairwise correlations as a function of their phylogenetic distance, revealing the emergence of a universal macroecological law. This law quantitatively states that the average correlation decays from positive to null values by increasing the phylogenetic distance, following a stretched-exponential decay function.

In this study we explored the possible ecological forces shaping species correlations. By scrutinizing different ecological models, each one implementing a diverse set of ecological forces, we found that the universal correlation pattern cannot be reproduced by competition or exclusion principles. Instead, temporal environmental filtering —i.e. the presence of correlated noise stemming from shared fluctuating factors— as modelled by a correlated stochastic-logistic model (CSLM), explains quantitatively empirical data. Furthermore, time-dependent (delayed) correlations in longitudinal data are also well reproduced by the model.

These results are based on multiple assumptions and their limitations give opportunities for extensions of the current work. First, at a theoretical level, the CSLM does not reproduce the distribution of correlations at each discrete phylogentic distance and, hence, neither the full distribution (see Fig.S22 in SI). The reason lies in the fact

that in order to be able to connect genetic and preference similarities, we enforce a "mean-field" type of relationship, Eq.(10), neglecting variability in the phenotypic-distance-to-preference-distance mapping. On the other hand, in figure S4 of the SI, we show that the variance of the distribution of pairwise correlations in each distance bin seems to follow a weak decaying power-law pattern with phylogenetic distance, with a diverse decaying exponent characteristic for each analyzed biome. Possibly, these patterns could be used to generate the preference vectors of the model in a more general way, allowing for more variability. Empirical data are not enough at the moment to proceed in this direction, and further analyses are required.

It is also important to stress that the origin of the power law behavior and its exponent value equal to 1/3 in the universal pattern of correlations (Eq.(1) remains unexplained. This scaling could be determined by the scale invariant, i.e. fractal, structure of phylogenetic trees[43–45], but further investigations, beyond the scope of the present work, are needed to shed light onto this empirical finding.

Although environmental filtering has been found to dominate the pattern of species-abundance correlations, the above mentioned variability could be the result of the complex interplay of other ecological forces. To identify which further forces are relevant and to discriminate their effects it will be important to analyze time-dependent data in a more detailed way as well as to analyze differences in carrying capacities, and correlations between different hosts [25]. At the modelling level, a more systematic study of the interplay between different ecological forces and how they impact the correlation spectrum at diverse resolution scales, is left for future work [46].

Another relevant caveat is that our analyses here are limited at the taxonomic resolution of OTUs, clustering together individuals with more than 97% similarity. Recent results suggest that ecological dynamics starts to decouple at much finer phylogenetic resolutions [47]. Morevoer, strains seem to still obey the three laws of variation and diversity valid at species level [48]. These result leave open the question on how ecological forces shape the variation of community composition at finer phylogenetic scales.

On the other hand, from a complementary viewpoint, we analyzed the behavior of correlations at the coarse-grained resolution of phyla. In particular, Fig. S7, in the SI illustrates that by considering just inter-phyla correlations one cannot observe the stretched exponential decay, that is determined by intra-phyla OTU pairs. Analogously, by extending our analysis to finer phylogenetic resolutions it could be possible to reveal the nature of intraspecific interactions, eventually showing the emergence of competition as a key player in determining correlations. Actually, our opinion is that, in order to have a more complete description of complex communities, one should not fix a characteristic taxonomic resolution, but, instead, start from individuals (or functional units) and progressively cluster them together at progressively more coarse-grained scales (i.e. moving across observational scales as customarily done in physics using "renormalization group" tools in statistical physics [49, 50]) as different ecological forces may shape communities at diverse resolution levels [51].

Data and Code

All the data sets analyzed in this work have been previously published and were obtained from the EBI Metagenomics database [41]. Previous publications of some of us have reported the original experiments and corresponding analyses [23]. In order to test the robustness of the macroecological laws and the modeling framework presented in this work, we considered 7 data sets that differ not only on the considered biome, but also on the sequencing techniques and

the pipelines used for data processing. Data sets were selected to represent a wide set of biomes. We considered only data sets with at least 50 samples with more than 10^4 reads. No data set was excluded a-posteriori. The main code used for analysis is available `here`.

Correlation analysis

In each community a, with $a = 1, .., M$, the count of the i-th species, with $i = 1, ..., N$, is called n_i^a and only sufficiently abundant species are considered, i.e., $N^a = \sum_{i=1}^{N} n_i^a \geq 10^4$. The relative abundance of species i in community a is calculated as:

$$x_i^a = \frac{n_i^a}{N^a}. \tag{11}$$

Community averages are defined as: $\langle .. \rangle = \frac{1}{M} \sum_{a=1}^{M} (..)$, such that the mean and the variance of a species relative abundance are:

$$\langle x_i \rangle = \sum_{a=1}^{M} \frac{x_i^a}{M}, \qquad Var_i = \langle x_i^2 \rangle - \langle x_i \rangle^2. \tag{12}$$

Another important quantity is the rank of species i in community a, r_i^a, where the most abundant species has rank $r_i^a = 1$, the second most abundant $r_j^a = 2$, and so on. Using these ingredients, one can construct the following (five) different quantities, that gauge fluctuations in species abundance, or simply "*fluctuation quantifiers*":

$$q_{1\,i}^a = \frac{x_i^a - \langle x_i \rangle}{\langle x_i \rangle} \tag{13}$$

$$q_{2\,i}^a = \frac{(n_i^a - N^a \langle x_i \rangle)}{N^a \langle x_i \rangle} \tag{14}$$

$$q_{3\,i}^a = \frac{x_i^a - \langle x_i \rangle}{\sqrt{Var_i}} \tag{15}$$

$$q_{4\,i}^a = \frac{\log x_i^a - \langle \log x_i \rangle}{\sqrt{Var(\log x_i)}} \tag{16}$$

$$q_{5\,i}^a = 2r_i^a - 1. \tag{17}$$

Similarly, one can estimate the correlation between species abundance fluctuations by using any of these quantifiers:

$$\eta_{k\,ij} = \langle q_{k\,i}^a q_{k\,j}^a \rangle_a = \sum_{a=1}^{M} \frac{q_{k\,i}^a q_{k\,j}^a}{M}, \tag{18}$$

for $k = 1, 2, ...5$. Finally, one can average over all pairs of species with a distance falling within a certain "bin" of phylogenetic distance.

Temporal analyses

The analysis of temporal (longitudinal) data is analogous to that for cross-sectional data in the preceding section, but instead of studying fluctuations and correlations between different communities, one considers a single community a data along a time-series (e.g. samples from different days of the time series, $t = 1, .., T$). All the quantities are defined

as above but replacing the community average by a time average $\langle .. \rangle_t = \frac{1}{T}\sum_{t=1}^{T}(..)$. In particular, the equal-time pairwise correlations are defined by:

$$\eta_{kij} = \langle q(t)_{k_i} q(t)_{k_j} \rangle_t = \sum_{t=1}^{T} \frac{q(t)_{k_i} q(t)_{k_j}}{T}; \tag{19}$$

for species i an j. Similarly, the Δt delayed correlation is:

$$\eta_{kij}(\Delta t) = \langle q(t+\Delta t)_{k_i} q(t)_{k_j} \rangle_t = \sum_{t=1}^{T-\Delta t} \frac{q(t+\Delta t)_{k_i} q(t)_{k_j}}{T}. \tag{20}$$

Models in preference space and evolutionary algorithm

In the preference space model, each single species is represented by a R-dimensional biotic (resource) preference vector $\boldsymbol{b}$ and a M-dimensional abiotic one $\boldsymbol{a}$. Without loss of generality, environmental factors are assumed to be equivalent and, in order to fix a tradeoff, the preference vectors of all species are assumed to have the same squared module, fixed to $r_P^2 > 0$, so that they can be characterized by a point in a R-dimensional sphere of radius r_P, i.e.: $|b|^2 = \sum_{\alpha=1,\dots R} b_\alpha^2 = r_P^2$ (respectively on a M-dimensional sphere with same radius in abiotic space).

Using the explicit expressions for the dynamics of biotic and abiotic factors, the general model as defined by Eq.(2), can be rewritten as the generalized Lotka-Volterra eqaution, Eq.(5), with deterministic growth rate and interaction matrix given by

$$\bar{r}_i \;=\; \bar{R}\sum_\beta b_\beta^i + \bar{M}\sum_\alpha a_\alpha^i \tag{21}$$

and

$$C_{ij} \;=\; \bar{R}\gamma \boldsymbol{b}^i \cdot \boldsymbol{b}^j \tag{22}$$

respectively, and with an effective zero-mean Gaussian noise:

$$\sqrt{\sigma}\xi_i(t) \;=\; \sqrt{\omega}\bar{R}\sum_\beta b_\beta^i \varphi_\beta + \sqrt{\nu}\bar{M}\sum_\alpha a_\alpha^i \zeta_\alpha \tag{23}$$

with covariance matrix given by Eq.(7), and the amplitude is $\sigma = \nu\bar{M}^2 + \omega\bar{R}^2$.

In all the variants of the model considered here (A, B and C) only on set of preference vector is needed (either biotic for models A and B, or abiotic for C). Thus, one can quantify the preference similarity or, simply, the "*preference distance*" between species i and j, as the cosine distance between their relevant preference vectors (for simplicity, in the following, we restrict the notation to model C for which abiotic preferences are relevant). The preference distance is defined as:

$$d_{P,ij} \equiv \frac{2}{\pi}\theta = \frac{2}{\pi}\arccos\left(\frac{\boldsymbol{a^i}\cdot\boldsymbol{a^j}}{|\boldsymbol{a^i}||\boldsymbol{a^j}|}\right) = \frac{2}{\pi}\arccos\left(\frac{\boldsymbol{a^i}\cdot\boldsymbol{a^j}}{r_P}\right), \tag{24}$$

where the subindex P stands either for "preference".

One can generate the set of M preference vectors $\boldsymbol{a}$ by sampling their component from a Gaussian with mean m/M (m small and positive) and standard deviation $1/\sqrt{M}$, $\mathcal{N}(m/M, 1/\sqrt{M})$, such that the radius is constant and close to unity for large values of M:

$$r_P^2 = \sum_\alpha a_\alpha^2 = 1 + \frac{m^2}{M} \approx 1. \tag{25}$$

However, as a consequence of the central limit theorem, for sufficiently large numbers of environmental factors, M, the random vectors $\boldsymbol{a^i}$ tend to be orthogonal to each other, i.e., $d_{P,ij} \approx 1 \quad \forall i,j$), hindering the possibility of generating similar species by simple random sampling. In order to circumvent this difficulty, we devised a simple evolutionary algorithm, such that, starting from an initial random distribution of vectors $\boldsymbol{a^i}^0$ —and implementing and evolutionary branching process— generates as an outcome a set of vectors $\boldsymbol{a^i}$ which are distributed across a broad range of possible cosine-distance values. The algorithm includes the following steps:

1. Sample at random two species i, j, j dies and i reproduces, making a copy (labeled j) of itself with some variation.

2. The preference vectors of the new species are obtained from the old one with some variation:

$$\boldsymbol{a^i} = q\boldsymbol{a^i} + (1-q)\boldsymbol{\epsilon}^i, \tag{26}$$

$$\boldsymbol{a^j} = q\boldsymbol{a^i} + (1-q)\boldsymbol{\epsilon}^j \tag{27}$$

   where the parameter $q \in [0,1]$ is the fidelity of reproduction and $\epsilon^{i,j}$ are vectors sampled from $\mathcal{N}(m/M, 1/\sqrt{M})$ (note that the resulting vectors are kept within the sphere).

3. Iterate Z times.

By considering a sufficiently large number of iterations Z and a value $q = 0.9$, the population develops a pool of similar individuals, with small pairwise distances, which was absent in the initial condition and covers, even if in an heterogeneous way, all the spectrum of possible distances (see Fig. S9 in the supplementary material).

Correlated stochastic logistic model

Derivation

The CSLM is obtained from Eq. (2) in the case where each species consumes only one resource with baseline $\bar{R}_i$ at rate γ_i and this resource is not consumed by any other species (model C). In particular, by taking the limit $M \gg 1$, one can easily find Eq.(8) with following definitions of the involved parameters:

$$\tau_i^{-1} = m(\bar{M} + \bar{R}_i) - \delta \tag{28}$$

$$K_i = \frac{m^2(\bar{R}_i + \bar{M}) - \delta}{m\bar{R}\gamma_i} \tag{29}$$

$$\sigma_i = \frac{\nu \bar{M}^2}{m(\bar{R}_i + \bar{M})} \tag{30}$$

$$\xi_i = \sqrt{\frac{\tau_i}{\sigma_i}} \sum_\alpha a^i_\alpha \zeta_\alpha(t) \tag{31}$$

The new environmental noise ξ_i is still Gaussian, because it is the weighted sum of Gaussian variables, with moments:

$$\langle \xi_i(t) \rangle = = 0 \tag{32}$$

$$\begin{aligned} \langle \xi_i(t)\xi_j(t) \rangle &= \sqrt{\frac{\tau_i \tau_j}{\sigma_i \sigma_j}} \sum_{\alpha,\beta=1}^{R} a^i_\alpha a^j_\beta \langle \zeta_\alpha(t)\zeta_\beta(t') \rangle \\ &= \boldsymbol{a^i} \cdot \boldsymbol{a^j} = \cos\left(\frac{\pi}{2} d_{P,ij}\right), \end{aligned} \tag{33}$$

where we have used the parameter definition Eq.(28), the normalization condition $|\boldsymbol{a^i}|^2 = 1$ and the definition of preference distance.

Macroecological laws and marginal properties

The CSLM, in the discretization scheme, has a Gamma stationary *marginal* distribution [23, 52]:

$$P^*(x_i) = \frac{1}{\Gamma(\beta_i)} \left(\frac{\beta_i}{\bar{x}_i}\right)^{\beta_i} x_i^{\beta_i - 1} \exp\left(-\beta_i \frac{x}{\bar{x}_i}\right), \tag{34}$$

where the average abundance $\bar{x}_i$ and the squared inverse coefficient of variation β_i read:

$$\bar{x}_i = K_i \left(1 - \frac{\sigma_i}{2}\right), \tag{35}$$

$$\beta_i := \frac{\bar{x}_i^2}{Var_i} = \frac{2}{\sigma_i}\left(1 - \frac{\sigma_i}{2}\right)^2, \tag{36}$$

respectively, coinciding with the ones obtained for the standard SLM [23]. Hence, the CSLM is able to reproduce the three macroecological laws for diversity and fluctuation, namely:

1. The stationary marginal distribution of species abundances is a Gamma distribution.
2. By fixing $\sigma_i = \sigma$, for all species the Taylor law relating the mean and variances across species is recovered.
3. The mean abundances are distributed as a log-normal just by imposing that the K_i's are log-normally distributed too.

Correlations

The joint probability cannot be calculated analytically for the CSLM, and hence an expression for the pairwise correlation functions cannot be derived in an exact way. Nevertheless, one can employ a linear-noise approximation around the fixed point (see SI. sec.2.4.2 for details) leading to:

$$\begin{aligned} \eta_{ij} &= \frac{\langle x_i x_j \rangle - \langle x_i \rangle \langle x_j \rangle}{\sqrt{Var_i Var_j}} = \frac{\exp\left(\cos\left(\frac{\pi}{2} d_{P,ij}\right)\left(\frac{\sigma}{2-\sigma}\right)\right) - 1}{\exp\left(\left(\frac{\sigma}{2-\sigma}\right)\right) - 1} \\ &\approx \cos\left(\frac{\pi}{2} d_{P,ij}\right), \end{aligned} \tag{37}$$

which is the expression employed in the main text to relate correlations with preference distances.

On the other hand, the Langevin equation of the model can be solved exactly, leading to:

$$x_i(t) = \frac{K_i \tau x_i(0) e^{(1-\frac{\sigma}{2})\frac{t}{\tau} + \sqrt{\frac{\sigma}{\tau}} W_i(t)}}{x_i(0) I_i[0,t] + K_i \tau}, \tag{38}$$

$$W_i(t) = \int_0^t ds \xi_i(s), \tag{39}$$

where $I_i[0,t]$ the integral of the associated Geometric Brownian motion:

$$I_i[0,t] = \int_0^t ds \exp\left((1 - \frac{\sigma}{2})\frac{s}{\tau} + \sqrt{\frac{\sigma}{\tau}} W_i(s)\right). \tag{40}$$

The exact integral Eq.(38) can be used to understand the effect of delays on pairwise correlations. Indeed, assuming that the system has reached the stationary state for sufficiently large times ($t \to \infty$), one can compute heuristically the relation between the abundance at time t and at a later time $t + \Delta t$:

$$\begin{aligned} x_i(t+\Delta t) &\approx K_i \tau e^{(1-\frac{\sigma}{2})\frac{t+\Delta t}{\tau} + \sqrt{\frac{\sigma}{\tau}} W_i(t+\Delta t)} I_i[0, t+\Delta t]^{-1} \\ &= x_i(t) \exp\left((1-\frac{\sigma}{2})\frac{\Delta t}{\tau}\right)\kappa(t, \Delta t), \end{aligned} \tag{41}$$

$$\kappa(t, \Delta t) = \exp\left(\sqrt{\frac{\sigma}{\tau}} \int_t^{t+\Delta t} \zeta_i(s)\right)\left(\frac{I_i[0,t]}{I_i[0, t+\Delta t]}]\right); \tag{42}$$

the function κ in the limit $t \gg \Delta t$ converges to 1, so that

$$x_i(t+\Delta t) \approx e^{(1-\frac{\sigma}{2})\frac{\Delta t}{\tau}} x_i(t). \tag{43}$$

Plugging this expression into the Pearson coefficient formula one readily obtains:

$$\eta_{ij}(\Delta t) \approx e^{(1-\frac{\sigma}{2})\frac{\Delta t}{\tau}} \eta_{ij}(0), \tag{44}$$

that combined with the linear approximation, Eq.(37), leads to:

$$\eta_{ij}(\Delta t) \approx e^{(1-\frac{\sigma}{2})\frac{\Delta t}{\tau}} \cos\left(\frac{\pi}{2} d_{P,ij}\right); \tag{45}$$

see SI. sec.2.4.3 for more details.

Inferring preference distance from data

To tune the CSLM to reproduce the observed empirical pattern it is necessary to infer the relation between preference and phylogenetic distances. Note that the empirical pattern we aim at reproducing is between average correlation and averaged phylogenetic distance within each bin, i.e., it suffices to find a relation between the (average) distance d_P and d_G (in other words: we are not interested in the full probability distribution of correlations in one bin, but just on its mean value).

The preference distance can be calculated by inverting the formula for the correlation Eq.(37) and by taking averages over the couples within each bin of phylogenetic distance:

$$\begin{aligned} d_P &= \frac{2}{\pi}\langle \arccos(\eta_{ij})\rangle_{ij} \approx \frac{2}{\pi}\arccos(\eta(d_G)) \\ &= \frac{2}{\pi}\arccos\left(e^{-\lambda d_G^{1/3}}\right), \end{aligned} \tag{46}$$

where the variance of η_{ij} within each bin of phylogenetic distance has been neglected, i.e. a so-called "mean-field approximation". A plot and a discussion of Eq.(46) can be found in the SI, sec. 2.6. Thanks to Eq.(46) it is possible to generate a preference-distance matrix, and hence the matrix of noise pairwise correlations from phylogenetic data:

$$d_{P,ij} = \frac{2}{\pi}\arccos\left(e^{-\lambda d_{G,ij}^{1/3}}\right) \tag{47}$$

$$\langle \xi_i(t)\xi_j(t')\rangle = \delta(t-t')e^{-\lambda d_{G,ij}^{1/3}}. \tag{48}$$

Clearly, this simple version of the CSLM cannot reproduce correlation variability as a function of phylogenetic similarity (see Discussion for possible extensions).

Simulations

The different models in preference space, Eq.(5) as well as the CSLM have been simulated in the Itô discretization scheme using the Milshtein algorithm [53] In Fig. 2, gray points stand for the Pearson's correlation coefficients at the stationary state for 10 realizations with $N = 200$ species and $M = R = 300$; the averages are obtained over 10^3 samples at stationarity, at time separated by $\delta_t = 10$. Red lines are obtained by averaging the correlation over pairs. In each simulation the initial populations are sampled from a Gaussian distribution $N(0.5, 0.01)$; other parameters are $N = 200, R = M = 300, m = 0.1, \bar{R}_i = \bar{M} = 0.1, \gamma_i = 1, \nu_\alpha = \omega_\alpha = 0.1, q = 0.9, Z = 50N, t_{fin} = 10^4$.
In Fig. 3 dark-green points stand for the Pearson's correlation coefficient at the stationary state of 10 realizations with $N = 300$ species, the averages are over 10^3 abundances sampled during the stationary time series every $\delta_t = 10\tau$. In each realization, we use the phylogenetic distances of N species sampled at random from the phylogenetic distance matrix of a random community of the considered biome to construct the species noises correlation, Eq.(47). The model parameters are set to reproduce the species marginal properties and delayed correlations, following the prescriptions from Sec.. Carrying capacities are generated log-normally by taking the exponential of random variables sampled from a Gaussian distribution $N(\bar{K}, \sigma_K)$, $\tau_i = \tau$ and $\sigma_i = \sigma$ for $i = 1, .., N$. Parameter values: $\tau = 1, \bar{K} = 16.1, \sigma_K = 3.8, \sigma = 1.42, \lambda = 3.5, t_f = 10^4$.

M.S., M.A.M and J.G. designed the research and wrote the manuscript. M.S and J.G. performed the analytical calculations, analyzed the data, and wrote the code. M.A.M. and M.S. acknowledge the Spanish Ministry and Agencia Estatal de investigación (AEI) through Project of I+D+i Ref. PID2020-113681GB-I00, financed by MICIN/AEI/10.13039/501100011033 and FEDER "A way to make Europe", as well as the Consejería de Conocimiento, Investigación Universidad, Junta de Andalucía and European Regional Development Fund, Project P20-00173 for financial support. We also thank J. Cuesta, J. Camacho Mateu, J. Iranzo, R. Rubio de Casas, L. Seoane for valuable discussions and/or suggestions on earlier versions of the manuscript.

[1] Whitman, W. B., Coleman, D. C. & Wiebe, W. J. Prokaryotes: The unseen majority. *Proceedings of the National Academy of Sciences* **95**, 6578–6583 (1998). URL https://www.pnas.org/content/95/12/6578. https://www.pnas.org/content/95/12/6578.full.pdf.

[2] Mandal, S. *et al.* Analysis of composition of microbiomes: a novel method for studying microbial composition. *Microbial ecology in health and disease* **26**, 27663 (2015).

[3] Frentz, Z., Kuehn, S. & Leibler, S. Strongly deterministic population dynamics in closed microbial communities. *Phys. Rev. X* **5**, 041014 (2015). URL https://link.aps.org/doi/10.1103/PhysRevX.5.041014.

[4] Ratzke, B. J., Christoph & Gore, J. Strength of species interactions determines biodiversity and stability in microbial communities. *Nature Ecology Evolution* **4**, 376–383 (2020). URL https://doi.org/10.1038/s41559-020-1099-4.

[5] Gralka, M., Szabo, R., Stocker, R. & Cordero, O. X. Trophic interactions and the drivers of microbial community assembly. *Current Biology* **30**, R1176–R1188 (2020). URL https://www.sciencedirect.com/science/article/pii/S0960982220311611.

[6] Friedman, J., Higgins, L. M. & Gore, J. Community structure follows simple assembly rules in microbial microcosms. *Nature Ecology &Evolution* **1** (2017).

[7] Szabo, R. E. *et al.* Ecological stochasticity and phage induction diversify bacterioplankton communities at the microscale. *bioRxiv* (2021). URL https://www.biorxiv.org/content/early/2021/09/27/2021.09.27.461956. https://www.biorxiv.org/content/early/2021/09/27/2021.09.27.461956.full.pdf.

[8] Goldford, J. E. *et al.* Emergent simplicity in microbial community assembly. *Science* **361**, 469–474 (2018).

[9] Kehe, J. *et al.* Positive interactions are common among culturable bacteria. *Science Advances* **7**, eabi7159 (2021).

[10] Ley, R. E., Lozupone, C. A., Hamady, M., Knight, R. & Gordon, J. I. Worlds within worlds: evolution of the vertebrate gut microbiota. *Nature Reviews Microbiology* **6**, 776–788 (2008).

[11] Thompson, L. *et al.* A communal catalogue reveals earth's multiscale microbial diversity. *Nature* **551**, 457–463 (2017).

[12] Lozupone, C. A. & Knight, R. Global patterns in bacterial diversity. *Proceedings of the National Academy of Sciences* **104**, 11436–11440 (2007). URL https://www.pnas.org/content/104/27/11436. https://www.pnas.org/content/104/27/11436.full.pdf.

[13] Arumugam, M. *et al.* Enterotypes of the human gut microbiome: [plus]corrigendum [plus]addendum. *Nature* **473**, 174–180 (2011).

[14] Grieneisen, L. *et al.* Gut microbiome heritability is nearly universal but environmentally contingent. *Science* **373**, 181–186 (2021). URL https://www.science.org/doi/abs/10.1126/science.aba5483. https://www.science.org/doi/pdf/10.1126/science.aba5483.

[15] Martiny, J. B. H., Jones, S. E., Lennon, J. T. & Martiny, A. C. Microbiomes in light of traits: A phylogenetic perspective. *Science* **350**, aac9323 (2015).

[16] Prosser, J. I. *et al.* The role of ecological theory in microbial ecology. *Nature Reviews Microbiology* **5**, 384–392 (2007).

[17] Marquet, P. A. *et al.* On Theory in Ecology. *BioScience* **64**, 701–710 (2014). URL https://doi.org/10.1093/biosci/biu098. https://academic.oup.com/bioscience/article-pdf/64/8/701/14094079/biu098.pdf.

[18] Gilbert, J. A. & Dupont, C. L. Microbial metagenomics: Beyond the genome. *Annual Review of Marine Science* **3**, 347–371 (2011). URL https://doi.org/10.1146/annurev-marine-120709-142811. PMID: 21329209, https://doi.org/10.1146/annurev-marine-120709-142811.

[19] Brown, J. H. *et al.* *Macroecology* (University of Chicago Press, 1995).

[20] Shade, A. *et al.* Macroecology to unite all life, large and small. *Trends in Ecology Evolution* **33**, 731–744 (2018). URL

https://www.sciencedirect.com/science/article/pii/S0169534718301861.

[21] Shoemaker, W. R., Locey, K. J. & Lennon, J. T. A macroecological theory of microbial biodiversity. *Nature Ecology &Evolution* **1** (2017).

[22] Ji, B. W., Sheth, R. U., Dixit, P. D., Tchourine, K. & Vitkup, D. Macroecological dynamics of gut microbiota. *Nature microbiology* **5**, 768–775 (2020).

[23] Grilli, J. Macroecological laws describe variation and diversity in microbial communities. *Nature communications* **11**, 1–11 (2020).

[24] Descheemaeker, L. & de Buyl, S. Stochastic logistic models reproduce experimental time series of microbial communities. *eLife* **9**, e55650 (2020). URL https://doi.org/10.7554/eLife.55650.

[25] Zaoli, S. & Grilli, J. A macroecological description of alternative stable states reproduces intra- and inter-host variability of gut microbiome. *Science Advances* **7**, eabj2882 (2021).

[26] Ho, P.-Y., Good, B. H. & Huang, K. C. Competition for fluctuating resources reproduces statistics of species abundance over time across wide-ranging microbiotas. *Elife* **11**, e75168 (2022).

[27] O'Dwyer, J. P. & Chisholm, R. A mean field model for competition: from neutral ecology to the red queen. *Ecology letters* **17**, 961–969 (2014).

[28] Grilli, J., Barabás, G., Michalska-Smith, M. J. & Allesina, S. Higher-order interactions stabilize dynamics in competitive network models. *Nature* **548**, 210–213 (2017).

[29] Wootton, J. T. Indirect effects in complex ecosystems: recent progress and future challenges. *Journal of Sea Research* **48**, 157–172 (2002).

[30] Webb, C. O., Ackerly, D. D., McPeek, M. A. & Donoghue, M. J. Phylogenies and community ecology. *Annual review of ecology and systematics* **33**, 475–505 (2002).

[31] HilleRisLambers, J., Adler, P. B., Harpole, W. S., Levine, J. M. & Mayfield, M. M. Rethinking community assembly through the lens of coexistence theory. *Annual review of ecology, evolution, and systematics* **43**, 227–248 (2012).

[32] Cadotte, M. W. & Tucker, C. M. Should environmental filtering be abandoned? *Trends in ecology & evolution* **32**, 429–437 (2017).

[33] Emerson, B. C. & Gillespie, R. G. Phylogenetic analysis of community assembly and structure over space and time. *Trends in ecology & evolution* **23**, 619–630 (2008).

[34] Poulin, R., Krasnov, B. R., Pilosof, S. & Thieltges, D. W. Phylogeny determines the role of helminth parasites in intertidal food webs. *Journal of Animal Ecology* 1265–1275 (2013).

[35] Krasnov, B. R. *et al.* Co-occurrence and phylogenetic distance in communities of mammalian ectoparasites: limiting similarity versus environmental filtering. *Oikos* **123**, 63–70 (2014).

[36] Pérez-Valera, E. *et al.* Fire modifies the phylogenetic structure of soil bacterial co-occurrence networks. *Environmental Microbiology* **19**, 317–327 (2017).

[37] Cavender-Bares, J., Kozak, K. H., Fine, P. V. & Kembel, S. W. The merging of community ecology and phylogenetic biology. *Ecology letters* **12**, 693–715 (2009).

[38] Jeraldo, P. *et al.* Quantification of the relative roles of niche and neutral processes in structuring gastrointestinal microbiomes. *Proceedings of the National Academy of Sciences* **109**, 9692–9698 (2012).

[39] O'Dwyer, J. P., Kembel, S. W. & Green, J. L. Phylogenetic diversity theory sheds light on the structure of microbial communities. *PLoS computational biology* **8**, e1002832 (2012).

[40] Johnson, J. *et al.* Evaluation of 16s rrna gene sequencing for species and strain-level microbiome analysis. *Nature Communications* **10** (2019).

[41] Mitchell, A. *et al.* Ebi metagenomics in 2017: Enriching the analysis of microbial communities, from sequence reads to assemblies. *Nucleic acids research* **46** (2017).

[42] Laherrére, J. & Sornette, D. Theoretical microbial ecology without species. *The European Physical Journal B* **2**, 525â539 (1998). URL https://doi.org/10.1007/s100510050276.

[43] Burlando, B. The fractal dimension of taxonomic systems. *Journal of Theoretical Biology* **146**, 99–114 (1990). URL https://www.sciencedirect.com/science/article/pii/S0022519305800463.

[44] Hernandez-Garcia, E., Tugrul, M., Herrada, E., EguÃluz, V. & Klemm, K. Simple models for scaling in phylogenetic trees. *International Journal of Bifurcation and Chaos* **10**, 805–811 (2010).

[45] Xue, C., Liu, Z. & Goldenfeld, N. Scale-invariant topology and bursty branching of evolutionary trees emerge from niche construction. *Proceedings of the National Academy of Sciences* **117**, 7879–7887 (2020). URL https://www.pnas.org/content/117/14/7879. https://www.pnas.org/content/117/14/7879.full.pdf.

[46] Camacho Mateu, J., Sireci, M., Lampo, A., Cuesta, J. A. & Muñoz, M. A. Correlations and the forces shaping coexstince in models ecosystems (In preparation).

[47] Goyal, A., Bittleston, L. S., Leventhal, G. E., Lu, L. & Cordero, O. X. Interactions between strains govern the eco-evolutionary dynamics of microbial communities. *bioRxiv* (2021). URL https://www.biorxiv.org/content/early/2021/01/04/2021.01.04.425224. https://www.biorxiv.org/content/early/2021/01/04/2021.01.04.425224.full.pdf.

[48] Wolff, R., Shoemaker, W. & Garud, N. Ecological stability emerges at the level of strains in the human gut microbiome. *bioRxiv* (2021). URL https://www.biorxiv.org/content/early/2021/10/01/2021.09.30.462616. https://www.biorxiv.org/content/early/2021/10/01/2021.09.30.462616.full.pdf.

[49] Wilson, K. G. Problems in physics with many scales of length. *Scientific American* **241**, 158–179 (1979).

[50] Efrati, E., Wang, Z., Kolan, A. & Kadanoff, L. P. Real-space renormalization in statistical mechanics. *Reviews of Modern Physics* **86**, 647 (2014).

[51] Tikhonov, M. Theoretical microbial ecology without species. *Phys. Rev. E* **96**, 032410 (2017). URL https://link.aps.org/doi/10.1103/PhysRevE.96.032410.

[52] Faust, K. *et al.* Signatures of ecological processes in microbial community time series. *Microbiome* **6**, 1–13 (2018).

[53] Toral, R. & Colet, P. *Stochastic Numerical Methods: An Introduction for Students and Scientists* (Wiley-Vch, 2014).